RSC Advances

This is an *Accepted Manuscript*, which has been through the Royal Society of Chemistry peer review process and has been accepted for publication.

Accepted Manuscripts are published online shortly after acceptance, before technical editing, formatting and proof reading. Using this free service, authors can make their results available to the community, in citable form, before we publish the edited article. This *Accepted Manuscript* will be replaced by the edited, formatted and paginated article as soon as this is available.

You can find more information about *Accepted Manuscripts* in the Information for Authors.

Please note that technical editing may introduce minor changes to the text and/or graphics, which may alter content. The journal's standard Terms & Conditions and the Ethical guidelines still apply. In no event shall the Royal Society of Chemistry be held responsible for any errors or omissions in this *Accepted Manuscript* or any consequences arising from the use of any information it contains.

ROYAL SOCIETY OF CHEMISTRY

www.rsc.org/advances

Graphical abstract

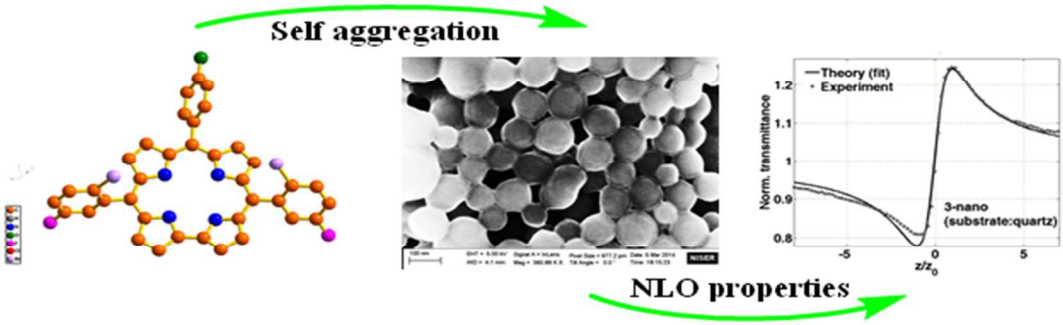

The NLO properties of a series of FB corroles are studied in the solution as well as in the aggregated state (in the form of thin films).

RSC Advances Accepted Manuscript

Cite this: DOI: 10.1039/c0xx00000x

www.rsc.org/xxxxxx

ARTICLE TYPE

A comparative study of optical nonlinearities of *trans*- A_2B-corroles in solution and in aggregated state

Antara Garai,[a] Samir Kumar,[b] Woormileela Sinha,[a] Chandra Shekhar Purohit,[a] Ritwick Das*[,b] and Sanjib Kar*[,a]

Received (in XXX, XXX) Xth XXXXXXXXX 20XX, Accepted Xth XXXXXXXXX 20XX
DOI: 10.1039/b000000x

A series of novel A_3-corrole and *trans*- A_2B-corroles have been synthesized with the aim of developing organic materials with improved nonlinear optical (NLO) properties. All the three newly synthesized corroles have been characterized by various spectroscopic techniques including single crystal X-ray structural analysis of the representative one. The crystal structure analysis of 10-(4-hydroxyphenyl)-5,15-bis(2-bromo-5-fluorophenyl) corrole, shows several O─H...N interactions. The self aggregates of all the three corroles were prepared on a silicon wafer as well as on quartz substrate by using drop-casting method in a dichloromethane and methanol (1:2) solvent mixture. In all the three free base corroles, well defined and nicely organized three-dimensional objects with diameter of ca. 320 nm (nanospheres), 450 nm (nanobulbs), and 120 nm (nanodiscs) were obtained. The NLO properties (nonlinear refractive index, n_2 and two-photon absorption coefficient, β) of all the corrole derivatives in toluene solution and as aggregated form were measured by Z-Scan technique. The nonlinear refractive indices, n_2 of the free base corroles (in toluene solution) were found out to be -16.8×10^{-18} m^2/W, -7.8×10^{-18} m^2/W and -25.9×10^{-18} m^2/W respectively and for the corresponding aggregates (nanoparticles of the free base corroles), it was found out to be -1.1×10^{-15} m^2/W, -1.9×10^{-15} m^2/W, and 71.8×10^{-15} m^2/W respectively. Similarly, the two-photon absorption coefficient, β of all the synthesized free base corroles (in toluene solution) were found out to be 5.7×10^{-15} m/W, 1.9×10^{-15} m/W and 17.2×10^{-15} m/W respectively and for the corresponding aggregates (nanoparticles), the values were 4.0×10^{-13} m/W, 2.0×10^{-13} m/W, and 444.0×10^{-13} m/W respectively. These NLO properties of the free base corrole derivatives (in solution and in aggregates) have been explored with a specific aim to identify the possibility of their applications in ultrafast switching devices for use in high-speed fiber-optic communications and photonic integrated circuits.

Introduction

Molecules with large nonlinear optical (NLO) coefficients have found extensive applications in wide-range of optoelectronic devices and in fiber-optic communication systems in the form of switches and routers.[1-6] The NLO properties of various organic molecules in terms of nonlinear refractive index (n_2), nonlinear or two-photon absorption (β), electro-optic and thermo-optic manifestations, dispersion properties etc. are being widely investigated in order to achieve rapid and error-free switching and routing.[7-9] Among the organic NLO materials, π─conjugated organic molecules such as porphyrin based materials are in the fore front due to very large polarizable electron density and therefore, exhibit non-resonant and ultrafast NLO responses.[10-14] The NLO properties of a large number of porphyrin based macrocycles, such as, porphyrins, phthalocyanines, and π-extended porphyrins have been widely investigated.[10-13] Among these porphyrin based macro-cycles, corrole based materials have been rarely explored.[15-16] When compared to analogous porphyins, corroles are contracted version with one methine carbon less. [17] This structural change imparts smaller cavity size of corrole compared to analogous porphyrin derivatives.[17] Previous literature reports suggest that corrole has highly conjugated π-electron density and it shows different photophysical properties compared to its porphyrin counterpart. [18-20] Due to the clear superiority than its porphyrin analogues and also the discovery of a facile synthetic methodology of corrole synthesis generated a tremendous interest generated in the development of novel corrole based materials for various applications.[21-23] Only a few literature reports show the interesting NLO properties of corrole based systems. Rebane et al.[15] has observed for the first time that compared to porphyrin, corrole shows larger two-photon cross sections due to lack of inversion center. Rao et al.[16] has demonstrated the third-order

RSC Advances Accepted Manuscript

NLO properties for two free base corrole derivatives and their corresponding germanium and phosphorous complexes. To the best of our knowledge, all the existing literature reports are related to the measurement of NLO properties of A_3-corroles only, however no studies have yet been done regarding the measurements of relatively more complicated *trans*-A_2B-corrole systems. Although the NLO properties of corroles are more promising than its porphyrin analogues, there have been very few attempts made to obtain a comparative account on NLO properties of corroles in aggregated state in addition to its solution phase NLO properties. The present work describes the synthesis of one novel A_3-corrole and two novel *trans*- A_2B-corroles namely, 5,10,15-tris[3,4-(1,4-dioxan)phenyl]corrole, **1**, 10-[4-(chloroacetoxy)phenyl]-5,15-bis(2-bromo-5-fluorophenyl) corrole, **2**, and 10-(4-hydroxyphenyl)-5,15-bis(2-bromo-5-fluorophenyl) corrole, **3** (Scheme 1). Various oxygenated functional groups are incorporated in the peripheral phenyl rings of the free base corrole derivatives, keeping in mind that these substituents might influence the formation of different sized and shaped self assembled aggregates. Use of self assembled porphyrins/corroles based systems in the design of improved NLO materials are borne out from the fact that there exists an induced electronic interaction among the adjacent porphyrins/corroles molecules. Theoretical calculations have also predicted the enhanced values of NLO responses upon self aggregation.[6] Third order NLO responses are found to increase markedly as the electron density in the macrocycle adds on. Thus electron releasing groups at the peripheral phenyl rings of the macrocycles would be a better choice for the same. Thus a series of electron donating substituents (1, 4─dioxan, 4─chloroacetoxy, and hydroxy) at the *para*-position of the phenyl rings are introduced. [11]

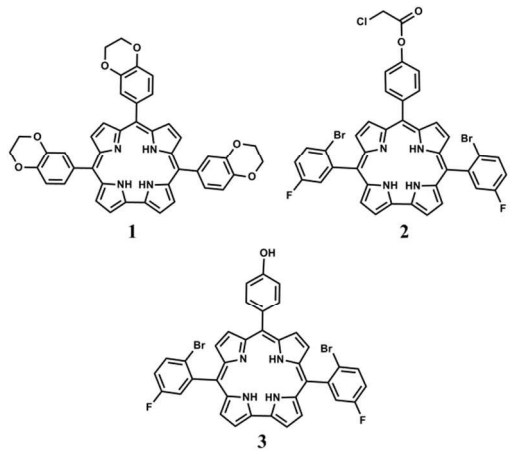

Scheme 1 Structure of the FB corroles 1─3

In addition to the synthesis and spectral characterization of **1**-**3**, the crystal structures of **3**, and NLO properties of **1**-**3** in solution state are also reported here. The present work also describes the synthesis of the aggregates of all the three FB (free base) corroles**.** In addition to the synthesis and characterization of the aggregates, the NLO properties of the aggregates are also studied and compared with the measurements in solution state.

Experimental section

Materials

The precursors pyrrole, 2-Bromo-5-fluorobenzaldehyde, DDQ (2,3-dichloro-5,6-dicyano-1,4-benzoquinone), and trifluoroacetic acid were purchased from Aldrich, USA. 4-hydroxybenzaldehyde, benzylamine, reagent grade THF, ethanol, dichloromethane, chloroacetylchloride, and triethylamine were purchased from Merck, India. Hexane and CH_2Cl_2 were distilled from KOH and CaH_2 respectively. For spectroscopic studies HPLC grade solvents were used.

Physical Measurements.

UV−Vis spectral studies were performed on a Perkin−Elmer LAMBDA-**750** spectrophotometer. Emission spectral studies were performed on a Perkin Elmer, LS 55 spectrophotometer using optical cell of 1 cm path length. The fluorescence quantum yields were determined using tetraphenylporphyrin, [TPP] as a reference.[18] Time resolved fluorescence measurements were carried out using a time-correlated single photon counting (TCSPC) spectrometer (Edinburgh, OB 920). The elemental analyses were carried out with a Perkin−Elmer 240C elemental analyzer. The NMR measurements were carried out using a Bruker AVANCE 400 NMR spectrometer. Chemical shifts are expressed in parts per million (ppm) relative to residual chloroform (δ= 7.26). Electrospray mass spectra were recorded on a Bruker Micro TOF─QII mass spectrometer. SEM images of the nanoparticles were captured by using a field emission gun scanning electron microscope (FEGSEM) (Zeiss, Germany make, Supra 55) equipped with energy-dispersive X-ray analysis system (EDAX). The ground state dipole moment of FB corrole derivatives **1**-**3** were calculated by the program package TURBOMOLE 6.4 using density functional theory (DFT) (see ESI†).

Crystal Structure Determination

Single crystals of **3** were grown by slow diffusion of a solution of the corrole in dichloromethane into hexane, followed by slow evaporation under atmospheric conditions. The crystal data of **3** was collected on a Bruker Kappa APEX II CCD diffractometer at 293 K. Selected data collection parameters and other crystallographic results are summarized in Table 1 and Fig. 1. All data were corrected for Lorentz polarization and absorption effects. The program package SHELXTL [24] was used for structure solution and full matrix least squares refinement on F^2. Hydrogen atoms were included in the refinement using the riding model. Contributions of H atoms for the water molecules were included but were not fixed. CCDC – 947032 contains the supplementary crystallographic data for **3**. These data can be obtained free of charge via www.ccdc.cam.ac.uk/data_request/cif.

NLO measurements.

The NLO properties (nonlinear refractive index, n_2 and two-photon absorption coefficient, β) of corrole derivatives **1**-**3** and aggregates of **1**-**3** (namely **1-Nano**, **2-Nano**, **3-Nano**) were

RSC Advances Accepted Manuscript

This journal is © The Royal Society of Chemistry [year]

measured using Z-Scan technique which employs an ultrafast laser source. Since, the absorption spectra revealed Q-band tails up to ~660 nm, we chose to measure the nonlinear response in the near-infrared region at a wavelength of 1064 nm so as to have minimal manifestation due to linear absorption and non-parametric effects. Our closed-aperture Z-scan set-up comprises a femtosecond (fs) Yb-fiber laser, delivering a linearly-polarized pulses of 250 fs at 80 MHz repletion rate at 1064 nm wavelength with maximum average output power of 5.0 W as shown in Fig. S1 (see ESI†). For varying the irradiance, we used a combination of half-wave plate (HWP) and polarizing beam splitter (PBS) after the isolator. Via this configuration, we vary the pulse energy of incident radiation varies from 1.2 nJ to 12 nJ. It is important to note that the fiber laser architecture ensures that the output power is delivered in TEM_{00} mode with $M^2 \leq 1.08$. This is an extremely crucial aspect of Z-Scan technique which essentially allows Gaussian-beam decomposition (GD) method to be employed for ascertaining the nonlinear refractive index (n_2) and nonlinear absorption (β) simultaneously as described below[1,2]. The output pulses were focused using a combination of diverging lens (f = –100 mm) and converging lens (f = +100 mm) resulting in a beam waist varying between 30±1 μm ≤w_0 ≤ 50±1 μm. 0.1 mM solutions of corrole derivatives **1-3** in toluene were prepared and a 1.0 mm thick cuvette carrying the solution was mounted on a motorized translation stage (10.0 cm travel) thus, ensuring that the sample translation is more than 25 times of the Rayleigh range (z_0) along the path of beam. The transmitted beam intensity was recorded in a photodetector after passing through an aperture of transmittance 'S'. Following an identical procedure, the closed-aperture Z-scan measurements of aggregates of **1**-**3** i.e. **1-Nano**, **2-Nano**, **3-Nano** on a quartz substrate is carried out. It is to be mentioned that the nonlinear response of toluene and quartz plate were used as a standard for measuring n_2 and β of solutions and their aggregates respectively.

2,2'-((2-Bromo-5-fluorophenyl)methylene)bis(1H-pyrrole), 2a.

In a 100ml two-necked round-bottomed flask, 2 g of 2-bromo-5-fluorobenzaldehyde (9.85mmol) was dissolved in 13.7 mL of freshly distilled pyrrole (197mmol) and stirred for 20 min at room temperature. 151μl of TFA (1.97mmol) was added drop wise to this mixture. The reaction mixture was then stirred at room temperature under N_2 atmosphere. The color of the solution gradually changed to dark orange. It was then dissolved with dichloromethane and washed several times with dilute NaOH solution, water and finally with brine solution. Organic layer was dried over anhydrous Na_2SO_4. It was evaporated and finally purified by column chromatography (silica gel 100-200 mesh, EtOAC / Hexane) to yield white color solid materials as final product. Yield: 80% (2.5g). Anal. Calcd (found) for $C_{15}H_{12}BrFN_2$: C, 56.45 (56.57); H, 3.79 (3.69); N, 8.78 (8.87). ^{1}H NMR (400 MHz, $CDCl_3$) δ 7.964 (brs, 2 H), 7.54-7.51 (m, 1 H), 6.89 - 6.82 (m, 2 H), 6.73-6.71 (m, 2H), 6.19-6.18 (m, 2H), 5.88 (brs, 2H), 5.83 (singlet, 1H), (see ESI†, Fig. S2). ESI-MS: m/z = 319.00 [**2a**+H]$^+$ (319.0168 calcd for $C_{15}H_{13}BrFN_2$) (Fig. S3).

4-(Chloroacetoxy)benzaldehyde, 2b.

4-(Chloroacetoxy)benzaldehyde was prepared by following a literature procedure.[25]

5,10,15-Tris[3,4-(1,4-dioxan)phenyl]corrole, 1.

1 was prepared according to available procedures of corrole synthesis.[22-23] 0.820 g of 1, 4-benzodioxan-6-carboxaldehyde (5 mmol) and 697μl of pyrrole (10 mmol) were dissolved in 400 mL of (1:1) MeOH/H_2O mixture. HCl (36%, 4.25ml) was then added drop wise to this reaction mixture. The reaction mixture was kept at stirring for 3 h at room temp. During the course of the reaction, the reaction mixture was changed its color from orange to dark greenish brown. The reaction mixture was then extracted with $CHCl_3$; the organic layer was washed thrice with H_2O, dried by anhydrous Na_2SO_4, and filtered, and diluted to 300 mL with $CHCl_3$. Then 1.23 g of p-chloranil (5 mmol) was added, and the reaction mixture was refluxed for 1.5 h. The solvent was removed by rotary evaporation and the dark green colored crude product was purified by column chromatography through silica gel (100-200 mesh) column using 80% DCM and 20% hexane as eluent. Subsequent recrystallization (CH_2Cl_2/hexane) gave the pure free base corrole, **1**. Yield: 18% (200mg). Anal. Calcd (found) for $C_{43}H_{32}N_4O_6$ (**1**): C, 73.70 (73.54); H, 4.60 (4.47); N, 8.00 (7.86). λ_{max}/nm (ε/$M^{-1}cm^{-1}$) in dichloromethane: 418 (129000), 577 (17300), 620 (16800), 654 (14500) (Fig. 2). ^{1}H NMR (400 MHz, $CDCl_3$) δ 8.89 (brs, 4 H), 8.58 (brs, 4H), 7.86-7.81 (m, 4 H), 7.67 - 7.62 (m, 2 H), 7.29-7.20 (m, 3 H), 4.48 (brs, 12 H), 1.49 (brs, 2H),─1.90(brm, 1H) (see ESI†, Fig. S4). ESI-MS: m/z =701.23 [**1**+H]$^+$ (701.2322 calcd for $C_{43}H_{33}N_4O_6$) (Fig. S5). **1** displayed strong fluorescence at 676 nm (Fig. 2), with excited state life time of 2.00 ns (Fig. S6).

10-[4-(Chloroacetoxy)phenyl]-5,15-bis(2-bromo-5-fluoro phenyl) corrole, 2.

0.99 g of 4-(chloroacetoxy)benzaldehyde (0.5 mmol) and 318 mg of 2-bromo-5-fluorophenyldipyromethane (1 mmol) were dissolved in 60 mL of dichloromethane. Then 3μl of TFA (0.04mmol) was added and the reaction was stirred for 5 h. Then the reaction mixture was diluted with 150 mL of dichloromethane and DDQ (227 mg, 1.01mmol) in THF solution was added to it. The mixture was stirred for another 30 minutes. The mixture was evaporated and was subjected to column chromatography. After recrystallization from a mixture of DCM and hexane, it afforded a dark blue green color solid. Yield: 11% (46 mg). Anal. Calcd (found) for $C_{39}H_{23}Br_2ClF_2N_4O_2$ (**2**): C, 57.62 (57.53); H, 2.85 (2.71); N, 6.89 (6.75). λ_{max}/nm (ε/$M^{-1}cm^{-1}$) in dichloromethane: 409 (139100), 564(21 300), 607 (11500), 643 (6700) (Fig. 2). ^{1}H NMR (400 MHz, $CDCl_3$) δ 9.01 (d, J=4.1 Hz, 2 H), 8.61 (q, J=4.8 Hz, 4 H), 8.45 (d, J=4.1 Hz, 2 H), 8.29 - 8.13 (m, 2 H), 7.97 (dd, J=8.9, 5.4 Hz, 2 H), 7.85 (dt, J=8.5, 3.4 Hz, 2 H), 7.53 (d, J=8.5 Hz, 2 H), 7.38 (td, J=8.5, 3.1 Hz, 2 H), 4.48 (s, 2 H), 1.59 (brs, 2H), ─2.35(brm, 1H) (Fig. S7). ^{13}C NMR (101 MHz, $CDCl_3$) δ 166.2, 162.4, 159.9, 150.2, 142.1, 141.9, 140.1, 135.6, 135.6, 135.1, 133.9, 133.8, 131.0, 126.9, 126.9, 122.6, 122.5, 122.4, 122.3, 121.9, 121.9, 121.9, 121.8, 121.0, 120.1, 117.4,

RSC Advances Accepted Manuscript

117.2, 116.5, 112.9, 110.5, 41.2 (ESI†, Fig. S8). ESI-MS: *m/z* = 810.98 [**2**+H]$^+$ (810.9844 calcd for $C_{39}H_{24}Br_2ClF_2N_4O_2$)(Fig. S9). **2** displayed strong fluorescence at 654 nm (Fig. 2), with excited state life time of 0.43 ns (Fig. S6).

10-(4-Hydroxyphenyl)-5,15-bis(2-bromo-5-fluorophenyl) corrole, 3.

In a 100 mL round bottom flask, 35 mg of 10-(4-(2-chloroacetoxy)phenyl)-5,15-bis(2-bromo-5-fluorophenyl) corrole (0.043 mmol) and 47 µl of benzylamine (0.43mmol) were taken in a mixture of THF (5ml) and ethanol (5ml). The mixture was refluxed for an hour. Then it was evaporated and was subjected to column chromatography (silica gel 100-200 mesh, EtOAc / hexane). After recrystallisation from a mixture of DCM and hexane, it afforded a dark blue green color solid. Yield: 70% (22 mg). Anal. Calcd (found) for $C_{37}H_{22}Br_2F_2N_4O$ (**3**): C, 60.35 (60.53); H, 3.01 (3.20); N, 7.61 (7.77). λ_{max}/nm (ε/$M^{-1}cm^{-1}$) in dichloromethane: 410 (159000), 563 (24500), 608 (15600), 638 (11200) (Fig. 2). ^{1}H NMR (400 MHz, $CDCl_3$) δ 9.00 (d, *J*=4.2 Hz, 2 H), 8.68 - 8.54 (m, 4 H), 8.44(d, *J*=4.2 Hz, 2 H), 8.13 - 7.92 (m, 4 H),7.86 (dt, *J*=8.8, 3.2 Hz, 2 H), 7.37 (td, *J*=8.4, 3.1 Hz, 2 H), 7.21 - 7.07 (m, 2 H), ─0.35 (brs, 4 H) (Fig. S10). ^{13}C NMR (101 MHz, $CDCl_3$) δ 162.3, 159.8, 154.7, 142.0, 139.7, 135.6, 135.2, 135.1, 134.1, 133.8, 133.7, 131.1, 131.0, 127.0, 126.5, 122.6, 122.4, 121.8, 117.3, 117.0, 116.5, 116.4, 114.0, 112.5, 111.4 (ESI†, Fig. S11). ESI-MS: *m/z* = 735.0 [**3**+H]$^+$ (735.0128 calcd for $C_{37}H_{23}Br_2F_2N_4O$) (Fig. S12). **3** displayed strong fluorescence at 661 nm (Fig. 2), with excited state life time of 0.34 ns (Fig. S6).

Results and discussion

Synthesis and Characterization

Synthesis of FB corrole, **1,** was achieved by following a general synthetic procedure of corrole synthesis.[22-23] For the synthesis of FB corrole, **2,** a synthetic procedure developed by Gryko *et al.* was followed.[26] For this purpose, 4-(chloroacetoxy)benzaldehyde, **2b** was prepared by following a earlier reported synthetic protocol.[25] A dipyromethane derivative namely, 2,2'-((2-bromo-5-fluorophenyl)methylene)bis(1H-pyrrole),**2a** was also synthesized. In the next step, both the dipyromethane and the 4-(chloroacetoxy) benzaldehyde were reacted in presence of TFA in dichloromethane solvent and subsequent oxidation with DDQ resulted the formation of **2**. Synthesis of FB corrole, **3,** was achieved after the de-protection of chloroacetoxy group in **2** with the help of benzyl amine (Scheme 2). Purity and identity of all the three FB corroles are demonstrated by their satisfactory elemental analyses and by the electrospray mass spectra (see Experimental Section).

Structures

The crystal structure of the FB corrole, **3** is shown in Fig. 1. The crystal system is monoclinic and the unit cell has four corrole molecules. Important crystallographic parameters are presented in Table 1. Bond distances and angles agree well with the previously reported other FB corrole molecules.[27-30]

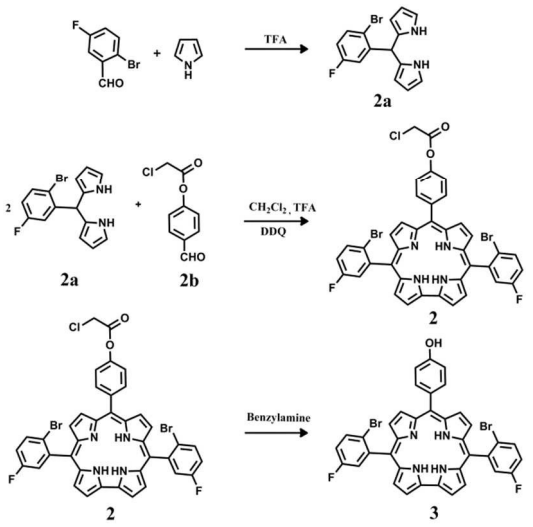

Scheme 2. Synthesis of 3

In the packing diagram of **3**, it has been observed that the inter-planar distance between the two corrole planes is ~3.51 Å. It appears that the two corrole molecules overlap appreciably with each other and forms sandwich type of configuration with two hydroxyphenyl groups of two different corrole units are *trans* to each other. In addition to the strong sandwich type of π-π stacking interactions mediated by the central aromatic rings, another kind of moderately strong parallel displaced π-π stacking interactions has also been observed among the corrole units through the phenyl rings at the *meso*- positions of corrole. The dihedral angles observed among the phenyl groups and the corrole ring are found to be 42.65°, 59.17°, and 67.84° and match well with those for analogous corrole derivatives.[26-30]The deviation observed among the pyrrole rings from the mean corrole plane range from ~8.03°─23.55°. The crystal structure analyses of **3** show several O─H...N interactions. The OH group of the hydroxyphenyl moiety of one corrole appears to undergo hydrogen-bonding with the amine and imine nitrogen atoms of other corrole ring. The shortest distance responsible for this kind of hydrogen bonding interactions is 2.86 Å [Bonding parameters of O–H···N; H···N: 2.129Å; O···N: 2.86 Å; ∠O–H···N: 148.3°]. This kind of hydrogen bonding interactions among the corrole units leads to supramolecular assemblies. Thus the solid state structure gets some extra stability due to the favorable intermolecular O─H...N interactions and extensive π-π stacking interactions (ESI†, Fig. S13).[26-30]

RSC Advances Accepted Manuscript

This journal is © The Royal Society of Chemistry [year]

Table 1 Crystallographic data for 3

Compound code	**3**
molecular formula	$C_{37}\ H_{22}\ Br_2\ F_2\ N_4\ O,\ 2CH_2Cl_2$
Fw	906.26
Radiation	MoKα
crystal symmetry	Monoclinic
space group	P 21/c
a(Å)	15.5405(10)
b(Å)	13.9867(9)
c(Å)	18.1492(13)
□(deg)	90
β(deg)	113.329(4)
□(deg)	90
V(Å^3)	3622.4(4)
Z	4
μ (mm^{-1})	2.583
T(K)	293(2) K
D_{calcd} (g cm^{-3})	1.662
2*θ* range (deg)	4.08 to 51.46
e data (R_{int})	6673 (0.1189)
R1 ($I>2\sigma(I)$)	0.0674
WR2 (all data)	0.1900
GOF	1.023
Largest diff. peak and hole(e·Å-3)	2.384 and -1.531

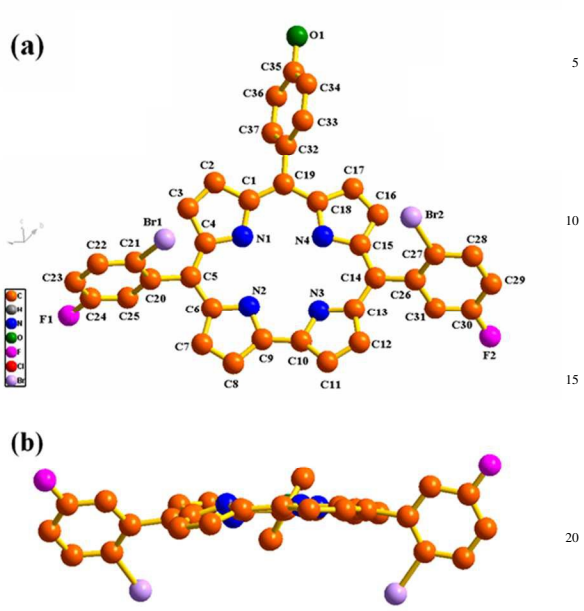

Fig. 1. Single-crystal X-ray structure of **3,** (a) top view (b) side view. Hydrogen atoms omitted for clarity.

Electronic Spectra

The electronic absorption spectral data of **1**-**3** in dichloromethane are presented in Table 2 (Fig. 2). The spectral profiles of these FB corroles can be easily explained with the help of Gouterman four-orbital model.[31] The Soret and Q-bands were observed at 418, 577, 620, and 654 nm respectively, for **1**, 409, 564, 607, and 643nm respectively, for **2**, and 410, 563, 608, and 638 nm respectively, for **3**.The observed band positions, spectral shapes and molar extinction coefficients of these corrole derivatives matched well with previously reported other corroles.[32-35]

Emission Spectra

The emission spectra of the compounds **1**-**3** in CH_2Cl_2 showed strong emissions in the red-region of the visible spectra. **1**-**3** displayed strong fluorescence with fluorescence maxima (□$_{max}$) at 676, 654, and 661 nm upon excitation at their respective Soret bands (Fig. 2, Table 2). The fluorescence lifetime of **1-3** were estimated to be 2.00, 0.43, and 0.34 ns respectively (Fig. S6, Table 2). The quantum yields of **1-3** were obtained as 0.16, 0.04, and 0.04 respectively (Table 2).

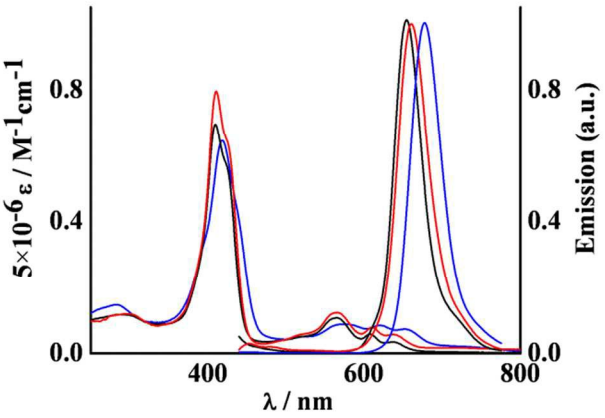

Fig. 2. Electronic absorption and normalized emission spectrum of **1,** (blue line), **2,** (black line), and **3**, (red line) in CH_2Cl_2 (Color online).

Table 2. Fluorescence data[a] of compounds 1-3.

Compound	Soret (nm)	Emission Maxima (nm)[b]	Φ_F[c]	τ (ns)
1	418	676	0.16	2.00
2	409	654	0.04	0.43
3	410	661	0.04	0.34

[a] In dichloromethane

[b]Excited at the Soret band.

[c]Quantum yields were calculated by following a standard protocol and by using H_2TPP as a reference compound.[18]

RSC Advances Accepted Manuscript

The spectral positions, shapes and decay profiles matched nicely with the previously reported other FB corrole derivatives. Earlier report also suggest that this kind of emission occurs from the lowest lying singlet excited state in the FB corrole derivatives.[36-37]

Self aggregates of 1─3

The self aggregates of all the three FB corroles were prepared on a silicon wafer as well as on a quartz substrate by using drop-casting method in a dichloromethane and methanol (1:2) solvent mixture. The generated aggregates were then examined by using SEM. The SEM images of the aggregates are shown in Fig.s 3, S14, and S15 respectively. Well defined and nicely organized three-dimensional objects with diameter of ca. 320 nm for **1** (Fig. S14), 450 nm for **2** (Fig. 4),

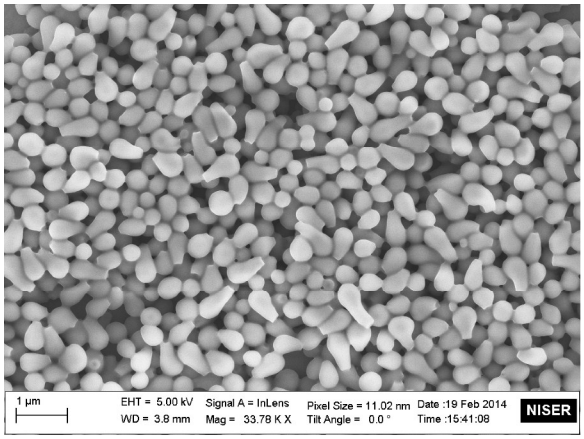

Fig. 3. SEM images of **2** revealed the formation of nanobulbs in dichloromethane─methanol mixture.

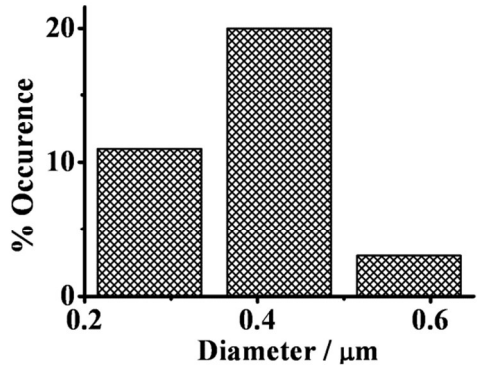

Fig. 4. Particle size distribution histograms of nanobulbs of **2** (extracted from Fig. 3).

and 120 nm for **3** (Fig. S16) were obtained. In case of corrole **1,** it was nanospheres, for **2**, it was nanobulbs, and for **3**, it was nanodiscs. The observed shapes of the aggregates of all the three FB corroles, **1-3,** can be correlated with the help of a model proposed by Srinivasarao et al.[38] This model predicts the formation of three dimensional objects in the drop casting method wherein a solvent/solvent-mixture is used to dissolve the solid materials provided that one of the solvent components must be denser than water and the material has a significant level of intermolecular interactions in the solid state. Single crystal X-ray structure analysis of **3** eventually supports the existence of a significant level of intermolecular interactions. It is highly likely that a similar type of intermolecular interactions also exists among the other two corrole molecules. The solute-solvent interaction ultimately changes the thermodynamics and the kinetics of the aggregation processes and leads to the generation of differently sized and shaped aggregates. [38-41] To analyze the composition of the nano-aggregates, EDAX analysis of the individual nanoparticles of FB corroles, **1-3**, were performed (Fig.s S17, S18, and S19, ESI†). All the constituent elements of **1-3** are present in those nanoparticles and their weight percentages are also very close to their actual weight percentages in the **1-3** molecules. It is worthwhile to mention here that in a dichloromethane and methanol (1:2) solvent mixture, there is no significant changes observed in the absorbance and emission spectra of the FB corroles **1-3** and so also in the dynamic light scattering (DLS) experiment in the solution phase (see ESI†).

Measurement of NLO properties

It is worthwhile to note that the thermo-optic effects such as thermal-lensing is always present due to high-repetition rate (80 MHz) of the fiber laser.[42-47]The onset of thermal-lensing is determined by a characteristic time (t_c) of the sample which is inversely proportional to its thermal diffusivity (D) and directly proportional to square of w_0.[40,45] Typically, $D \sim 10^{-7}$ m^2/s for organic solvents which results into $t_c \sim 1.0$ ms for beam waist varying between, $w_0 \sim 30$–50 µm. If the time-difference between the two consecutive pulses is less than t_c, the accumulated thermal energy (ATE) would manifest in the form of thermal-lens in the samples. Keeping this point in mind, we control the sample irradiation by chopping the incident laser beam by using custom-made chopper wheel with 0.83% duty cycle. The chopper frequency is set at 40 Hz which result in an effective laser repetition rate of 664 kHz. Fig. 5 (a-f) show the traces of normalized transmittance for **1-3** (0.1 mM solution in toluene) and **1-Nano**, **2-Nano**, **3-Nano** respectively as a function of z-axis translation for incident on-axis peak optical irradiances $I_0 \approx$ 1-4 GW/cm^2 (dotted curves). It is evident that the transmittance curves have symmetrically placed peak and valley and therefore, lies in the regime of small nonlinear phase-shift ($\Delta\varphi_0 \leq \pi$).[48,49]

Theoretical model for analyzing NLO responses

In order to ascertain the NLO parameters (n_2 and β) in presence of thermal nonlinearity such as thermal lensing, we employ the Gaussian decomposition (GD) technique after incorporating a non-local parameter (m). This idea was initially proposed by Ramirez *et al.*[48] so as to account for thermal effects. The inclusion of non-local term (m) brings in flexibility to consider spatial distribution of nonlinear phase-shift (φ) which can be wider as well as narrower than the incident Gaussian beam due to thermal contribution to optical nonlinearity. We consider a complex Gaussian beam (TEM_{00} mode) from a pulsed laser

RSC Advances Accepted Manuscript

This journal is © The Royal Society of Chemistry [year]

source to be incident on medium exhibiting $\chi^{(3)}$ nonlinearity. The complex field incident on the nonlinear medium is given by,[49]

$$E(r,z,t) = E_i(t)\frac{w_0}{w(z)}\exp\left(-\frac{r^2}{w^2(z)} - \frac{ikr^2}{2R(z)}\right)e^{-i\phi(z,t)} \quad \cdots (1)$$

where $w(z) = w_0/\left[1+(z/z_r)^2\right]^{1/2}$ is the beam radius at z (refer to ESI†, Fig. S1), $R(z) = z\left[1+(z_r/z)^2\right]^{1/2}$ is the radius of curvature, $z_0 = (1/2)kw_0^2$ is Rayleigh length for the focused Gaussian beam, $k = 2\pi n_0/\lambda = \omega_0/c$ is the wave number and E_i is the incident electric field amplitude in Eq. (1). Here, ω_0, λ are angular frequency, wavelength of *em* wave respectively and n_0 is linear refractive index of the sample. The term $e^{i\varphi(z,t)}$ contains all the radially uniform phase-variations and hence, does not play a significant role in analyzing self-focusing or self-defocusing effects. In presence of linear and nonlinear effects, the intensity at exit-plane of a thin sample of length L (<< z_0) is given by Eq. (2),[49]

$$I_e(z,r) = \frac{I_i(z,r)e^{-\alpha_0 L}}{1+q(z,r)} \quad \cdots\cdots (2)$$

where $I_i(z,r)$ represents the laser beam intensity at sample entrance plane, $q(z,r) = \beta I(z,r)L_{eff}$ is the normalized nonlinear absorption parameter and β is two-photon absorption coefficient. Here, α_0 is the linear absorption coefficient and $L_{eff} = \left(1-e^{-\alpha_0 L}\right)/\alpha_0$ is the effective length traversed by the beam in sample. By using the GD method, the nonlinear phase change is given by $\Delta\varphi(z,r) = \frac{kn_2}{\beta}ln[1+q(z,r)]$ where n_2 is nonlinear refractive index of the sample.[50-53] In order to account for non-local effects, nonlinear absorption parameter could be defined as given in Eq. (3) below.

$$q(z,r) = \frac{q_0}{1+(z/z_0)^2}exp\left(\frac{-2mr^2}{w^2(z)}\right) \quad \cdots (3)$$

where $q_0 = \beta I_0 L_{eff}$ with I_0 being the on-axis beam intensity at focus. The parameter '*m*' is defined as order of non-locality and can be any real positive number. For $m < 1$, the nonlinear phase change extends beyond the spatial incident intensity distribution whereas when $m > 1$, the nonlinear phase change is narrower than the spatial extent of incident intensity distribution. When $m = 1$, the nonlinear phase change has identical variation as that of incident intensity and the response can be considered as local. This would result in transmittance as given by Sheikh-Bahae *et al*.[49]

It is to be appreciated that $q(z)$ is usually very small, so that we can assume $\Delta\varphi(z,r) \approx \frac{kn_2}{\beta}q(z,r) = \Delta\varphi_0(z)exp\left(\frac{-2mr^2}{w^2(z)}\right)$ where $\Delta\varphi_0 = \frac{\Delta\Phi_0}{1+(z/z_0)^2}$. Here, $\Delta\Phi_0 = kn_2 I_0 L_{eff}$ which defines on-axis phase-shift at the focus due to refractive nonlinearity. Using the GD method and Eq. (1), the electric field at the sample exit plane is given by,[49, 53]

$$E_e(r,z) = E(r,z)e^{-\frac{\alpha_0 L}{2}}\sum_{n'=0}^{\infty}\left[\frac{(i\Delta\varphi_0(z))^{n'}}{n'!}\times\prod_{n=0}^{n'}\left(1-i(2n-1)\frac{\beta}{2kn_2}\right)\right] \quad \cdots (4)$$
$$\times exp\left(\frac{-2mn'r^2}{w^2(z)}\right)$$

By assuming that the field in Eq. (4) propagates to aperture plane undergoing only diffraction, the electric field at aperture plane can be written as shown in Eq. (5) below.

$$E_{out}(r,z) = E(r,z=0)e^{-\frac{\alpha_0 L}{2}}\sum_{n'=0}^{\infty}\left[\frac{(i\Delta\varphi_0(z))^{n'}}{n'!}\times\prod_{n=0}^{n'}\left(1-i(2n-1)\frac{\beta}{2kn_2}\right)\frac{w_{n'_0}}{w_{n'}}\right] \quad \cdots (5)$$
$$\times exp\left(\frac{-r^2}{w_{n'}^2} - \frac{ikr^2}{2R_{n'}} + i\theta_{n'}\right)$$

where $w_{n'_0}^2 = w^2(z)/(2n'+1)$, $d_{n'} = (1/2)kw_{n'0}^2$, $R_{n'} = d\left(1-\frac{g}{g^2+(d^2/d_{n'}^2)}\right)^{-1}$, $w_{n'}^2 = w_{n'0}^2\left(g^2+d^2/d_{n'}^2\right)$, $\theta_{n'} = \tan^{-1}\left(\frac{d/d_{n'}}{g}\right)$ and $g = 1+d/R(z)$. Here, '*d*' is the distance between sample exit plane and the aperture. Therefore, the normalized transmittance through a finite aperture of radius r_a would be given by the ratio of on-axis electric field in presence of nonlinear phase-shift and that in absence of any nonlinear effect i.e.

$$T(z,\Delta\varphi_0) = \frac{\left|E_{out}(z,r=0,\Delta\varphi_0)\right|^2}{\left|E_{out}(z,r=0,\Delta\varphi_0=0)\right|^2} \quad \cdots (6)$$

which can be simplified to obtain,[48,50]

$$T(z,\Delta\Phi_0,q_0) = 1 - \frac{4m\Delta\Phi_0 x + q_0(x^2(2m+1))}{(x^2+(2m+1)^2)(x^2+1)} \quad \cdots (7)$$

where $x = z/z_0$ and we have assumed that $d >> z_0$. Hence, Eq. (7) is used for obtaining 'n_2' and 'β' simultaneously from the experimentally measured normalized transmittance.

Results

Using the variation of normalized transmittance as shown in Fig.s 5(a)-(f) as well as Eq. (7), we obtained the values of nonlinear refractive index (n_2) and two-photon absorption coefficient (β) as shown in Table 3. It is apparent that the n_2 values of aggregates of **1-3** are about three orders of magnitude greater than that of solutions. Similarly, β for **1-Nano**, **2-Nano** and **3-Nano** exhibit about two orders of enhancement in magnitude as compared to the solutions. The obvious reason behind such an observation is an increase in overall density of molecules in solid aggregates as compared to their solutions. Due to higher density of molecules in aggregates in addition to low mobility in solid phase, the contribution to nonlinear optical effects is higher. Moreover, the solutions, namely **1-3** exhibit self-defocusing effect (negative n_2) in addition to positive nonlinear absorption (β). Usually, such a behavior is expected in solutions due to reduction in local density at high beam intensities which result in a negative (concave) lensing behavior. It was also observed that **1-Nano** and **2-Nano** defocuses the incident laser beam whereas **3-Nano** exhibits a self-focusing effect. Such a behavior clearly indicates that the impact of electrostriction in **3-Nano** masks other effects such as thermal lensing, photochemical ablation at femtosecond laser intensities, thereby resulting in positive-lensing behavior.[54]

RSC Advances Accepted Manuscript

Table 3. UV–Vis data [a] and NLO coefficients. [a,b]

Compound	UV–Vis data [a] λ_{max} / nm (ε/$M^{-1}cm^{-1}$)	n_2($\times10^{-18}$ m^2/W)	β (GM)	β ($\times10^{-15}$ m/W)
1[a]	421 (132000), 574 (15000), 620 (14250), 654 (11000).	–16.8	176	5.7
2[a]	412 (119000), 565 (20000), 610 (9000), 643 (4000).	–7.8	59	1.9
3[a]	410 (162500), 565 (24000), 612 (14000), 643 (11000).	–25.9	534	17.2
1-Nano	—	-1.1×10^3	–	4.0×10^2
2-Nano	—	-1.9×10^3	–	2.0×10^2
3-Nano	—	71.8×10^3	–	444×10^2

[a] In toluene

[b] λ_{ex} = 1064 nm

Although, molecules **2** and **3** resemble each other closely, the small nonlinear response as well as earlier onset of thermal effects at repetition rates ≥ 1 kHz in **2-Nano,** results in a self-defocusing behavior in aggregate phase. It is worthwhile to note that the nonlinear response (n_2 and β) of **3-Nano** are significantly higher as compared to other samples under study and the values are reasonable higher compared to related materials reported in literature (Table S1; ESI†).[55-60] For example, the two-photon absorption coefficient (β) for **3- Nano** is more than 100 times greater in magnitude as compared to **1-Nano** and about 200 times than that for **2-Nano**. The two-photon absorption cross-sections of different meso-substituted A_3-corroles were extensively studied by Rebane et al.[15] They have observed values of 60–130 GM. Osuka et al. have studied the corrole dimers and have obtained values of 1100– 4600 GM.[55] Rao et al. have studied the germanium and phosphorus corroles and have obtained values of 100–5400 GM.[16] In our case we have obtained values of 60-550 GM in solution phase measurement. A closer look reveals that our values are also in line with the previously reported data in solution phase measurement. However absorption cross-sections were never measured in corrole aggregates. The values obtained by us in the aggregated sate are 100-1000 times higher in comparison to the values obtained in solution. In general polarizability and ground state dipole moment dictates the NLO responses. The molecular ground state dipole moment has been calculated by using the DFT calculations (Fig. S20). The values obtained are in the same order of magnitudes (3.05, 1.67, and 2.45 Debye respectively for the FB corroles **1**-**3**). The large improvement of nonlinear optical behavior for **1-Nano**, **2-Nano** and **3-Nano** could be attributed due to the presence of coupled MOs and thus resulting in an enhanced transition dipole moment.

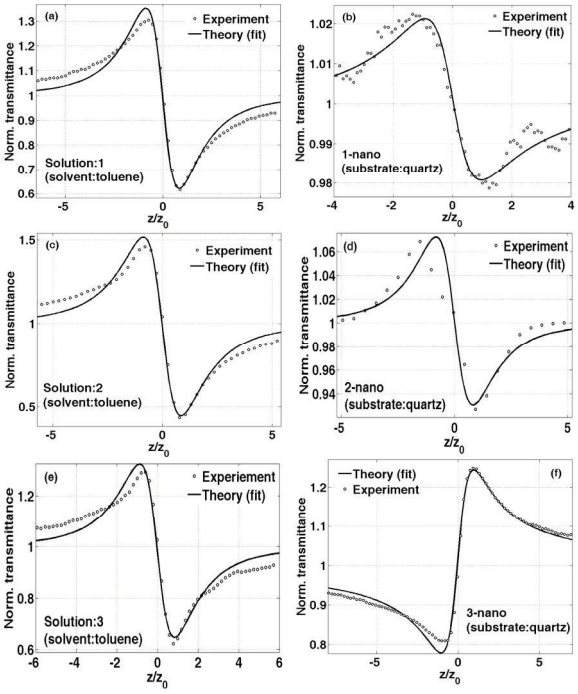

Fig. 5. Closed aperture normalized transmittance as a function of propagation distance (z) for (a) 0.1 mM solution **1** (in toluene) (b) Aggregates of **1** (**1**-Nano on quartz substrate) (c) 0.1 mM solution of **2** (in toluene) (d) Aggregates of **2** (**2**-Nano on quartz substrate) (e) 0.1 mM solution of **3** (in toluene) (f) Aggregates of **3** (**3**-Nano on quartz substrate).

Conclusions

The present work describes the synthesis of one novel A_3-corrole and two novel *trans*- A_2B-corroles. Purity and identity of all the three FB corroles are demonstrated by various spectroscopic techniques. The crystal structure analysis of the FB corrole, **3** are also described. Extensive intermolecular O─H...N interactions and π-π stacking interactions are observed in the single crystal X-ray structural analysis the FB corrole **3**. The self aggregates of all the three corroles were generated on a silicon wafer as well as on quartz substrate by using drop-casting method in a dichloromethane and methanol (1:2) solvent mixture. The generated aggregates were then examined by using SEM techniques. The NLO properties of FB corroles; **1**-**3** are studied in the solution as well as in the aggregated state (in the form of thin films). The results show that the nonlinear refractive index, n_2, as well as two-photon absorption coefficient (β) of corrole **3** (in toluene solution) and its solid aggregates (**3-Nano**) are significantly greater than that of corroles **1** and **2**. Our study indicates that the corrole-**3** and **3-Nano** are promising candidates

RSC Advances Accepted Manuscript

This journal is © The Royal Society of Chemistry [year]

(Table S1) for devising optical switches which can have direct applications in high-speed communication technology.

Acknowledgements

Financial support received from the Department of Atomic Energy, (India) is gratefully acknowledged. Authors thankfully acknowledge NISER-Bhubaneswar for providing infrastructure and instrumental supports. We would like to acknowledge Dr. H. S. Biswal for DFT calculations.

Notes and references

[a]*School of Chemical Sciences, National Institute of Science Education and Research (NISER), Bhubaneswar – 751005, India. E-mail: sanjib@niser.ac.in*

[b]*School of Physical Sciences, National Institute of Science Education and Research (NISER), Bhubaneswar – 751005, India. E-mail: ritwick.das@niser.ac.in*

† Computational details, Aggregation properties of **3**, X-ray single crystal structure analysis, ESI- MS spectrum, ^{1}H NMR, ^{13}C NMR spectrum, Beam profile of the transmitted beam, Scanning electron microscope (SEM) image, DFT optimized structures of 1─3, and crystallographic information file (CIF). CCDC–947032 contains the supplementary crystallographic data for 3. These data can be obtained free of charge via www.ccdc.cam.ac.uk/data_request/cif.

1 P. N. Prasad and D.J. Williams, Wiley: New York,USA 1990

2 G. C. Baldwin, Plenum, New York, USA 1996

3 B. J. Coe, M. C. Chamberlain, J. P. Essex-Lopresti, S. Gaines, J. C. Jeffery, S. Houbrechts and A. Persoons, *Inorg. Chem.,* 1997**, 36**, 3284-3292.

4 I. R. Whittall, A. M. McDonagh, M. G. Humphrey and M. Samoc *Advances in organometallic chemistry,* 1998**, 42**, 291-362.

5 A. M. McDonagh, M. G. Humphrey, M. Samoc, B. Luther-Davies, S. Houbrechts, T. Wada, H. Sasabe and A. Persoons, *J. Am. Chem. Soc.,* 1999**, 121**, 1405-1406.

6 A. Karotki, M. Drobizhev, Y. Dzenis, P.N. Taylor, H.L. Anderson and A. Rebane, *Phys. Chem. Chem. Phys.,* 2004**, 6**, 7-10.

7 B. E. A. Saleh and M. C. Teich, Wiley, New York, USA 1991.

8 R. A. Hann and D. Bloor, Royal Society of Chemistry, London, UK:1991

9 G. J. Ashwell and D. Bloor, Royal Society of Chemistry: 1993.

10 R. P. Linstead, *J. Chem. Soc.,* 1934, 1016-17.

11 K. M. Kadish, K. M. Smith and R. Guilard, The Porphyrin Handbook, Eds. Academic, New York, USA: 2003.

12 K. S. Suslick, C. T. Chen, G. R. Meredith and L. T. Cheng, *J. Am. Chem. Soc.,* 1992**, 114**, 6928-30.

13 M. O. Senge, M. Fazekas, E. G. A. Notaras, W. J. Blau, M. Zawadzka, O. B. Locos and E. M. N. Mhuircheartaigh, *Adv. Mater. (Weinheim, Ger.)* 2007**, 19**, 2737-2774.

14 D. S. Chemla, J. Zyss, Chemla, D. S. Zyss, J., Eds. Academic, Orlando, USA 1987; Vol. I and II.

15 A. Rebane, M. Drobizhev, N. S. Makarov, B. Koszarna, M. Tasior and D. T. Gryko, *Chem. Phys. Lett.*, 2008**, 462**, 246-250.

16 P. T. Anusha, D. Swain, S. Hamad, L. Giribabu, T. S. Prashant, S. P. Tewari and S. V. Rao, *J. Phys. Chem. C,* 2012*,* **116***, 17828-17837.*

17 R.Guilard, J.-M. Barbe, C.Stern, K. M. Kadish, The Porphyrin Handbook. K. M. Kadish, K. M. Smith and R. Guilard, Eds. Elsevier Science, USA: 2000.

18 T. Ding, E. A. Alemán, D. A. Modarelli and C. J. Ziegler, *J. Phys. Chem. A*, 2005**, 109**, 7411-7417.

19 B. Ventura, A. Degli Esposti, B. Koszarna, D. T. Gryko and L. Flamigni, *New J. Chem.,* 2005**, 29**, 1559-1566.

20 L. Flamigni, B. Ventura, M. Tasior, T. Becherer, H. Langhals and D. T. Gryko, *Chem.Eur.J.,* 2008, **14**, 169-183.

21 I. Aviv and Z. Gross, *Chem. Commun. (Cambridge, U. K.),* 2007**, 20**, 1987-1999.

22 B. Koszarna and D. T. Gryko, *J. Org. Chem.*, 2006**, 71**, 3707-3717.

23 R. Paolesse, A. Marini, S. Nardis, A. Froiio, F. Mandoj, D. J. Nurco, L. Prodi, M. Montalti and K. M. Smith, *J. Porphyrins Phthalocyanines,* 2003**, 7**, 25-36.

24 G. M. Sheldrick, *Acta Crystallogr., Sect. A: Found. Crystallogr.*, 2008**, 64** (1), 112-122.

25 J.-M. Barbe, G. Canard, S. Brandès and R. Guilard, *Eur. J. Org. Chem.*, 2005**, 21**, 4601-4611.

26 D. T. Gryko and K. Jadach, *J. Org. Chem.,* 2001**, 66**, 4267-4275.

27 S. Will, J. Lex, E. Vogel, H. Schmickler, J.-P. Gisselbrecht, C. Haubtmann, M. Bernard and M. Gorss, *Angew. Chem., Int. Ed. Engl.,* 1997**, 36**, 357-361.

28 R. Guilard, C. P. Gros, J.-M. Barbe, E. Espinosa, F. Jérôme, A. Tabard, J.-M. Latour, J. Shao, Z. Ou and K. M. Kadish, *Inorg. Chem.,* 2004**, 43**, 7441-7455.

29 W. Sinha, N. Deibel, H. Agarwala, A. Garai, D. Schweinfurth, C. S. Purohit, G. K. Lahiri, B. Sarkar and S. Kar, *Inorg. Chem.,* 2014*,* **53***, 1417-1429.*

30 A. M. Albrett, K. E. Thomas, S. Maslek, A. Młodzianowska, J. Conradie, C. M. Beavers, A. Ghosh and P. J. Brothers, *Inorg. Chem.,* 2014, **53**, 5486–5493

31 M. Gouterman, G. Wagniere and L. R. Snyder, *J. Mol. Struct.,* 1963, **11**, 108−127.

32 B. Koszarna and D. T. Gryko, *Chem. Commun.,* 2007**, 28**, 2994-2996.

33 W. Sinha, M. G. Sommer, N. Deibel, F. Ehret, B. Sarkar and S. Kar, *Chem. - Eur. J.,* 2014, **20**, 15920 – 15932

34 W. Sinha and S. Kar, *Organometallics,* 2014, **33**, 6550−6556

35 J. Rochford and E. Galoppini, *Langmuir,* 2008**, 24**, 5366-5374.

36 D. T. Gryko and B. Koszarna, *Organic & biomolecular chemistry,* 2003**, 1**, 350-357.

37 J.-P. Strachan, S. Gentemann, J. Seth, W. A. Kalsbeck, J. S. Lindsey, D. Holten and D. F. Bocian, *J. Am. Chem. Soc.,* 1997**, 119**, 11191-11201.

38 M. Srinivasarao, D. Collings, A. Philips and S. Patel, *Science,* 2001**, 292**, 79-82.

39 O. Valdes-Aguilera and D. C. Neckers, *Acc. Chem. Res*., 1989,**22**, 171-7.

40 E. H. Hill, D. Sanchez, D. G. Evans and D. G. Whitten, *Langmuir*, 2013, **29**, 15732-15737.

41 W. F. Mooney and D. G. Whitten, *J. Am. Chem. Soc.,* 1986**, 108**, 5712-19.

42 M. Falconieri and G. Salvetti, *Appl. Phys. B: Lasers Opt.,* 1999**, 69**, 133-136.

43 M. Gedikpinar, M. Cavas, Z. A. Alahmed and F. Yakuphanoglu, *Superlattices Microstruct.*, 2013, **59**, 123-132.

44 A. Gnoli, L. Razzari and M. Righini, *Opt. Express,* 2005**, 13**, 7976-7981.

45 R. d. Nalda, R. d. Coso, J. Requejo-Isidro, J. Olivares, A. Suarez-Garcia, J. Solis and C. N. Afonso, *J. Opt. Soc. Am. B,* 2002**, 19**, 289-296.

46. K. Kamada, K. Matsunaga, A. Yoshino and K. Ohta, *J. Opt. Soc. Am. B,* 2003**, 20**, 529-537.

RSC Advances Accepted Manuscript

47 C. Huang, Y. Li, Y. Song, Y. Li, H. Liu and D. Zhu, *Adv. Mater.,* 2010**, 22**, 3532-3536.

48 E. V. Garcia Ramirez, M. L. Arroyo Carrasco, M. M. Mendez Otero, E. Reynoso Lara, S. Chavez-Cerda and M. D. Iturbe Castillo, *J. Opt.,* 2011, **13**, 085203

49 M. Sheik-Bahae, A. A. Said, T. H. Wei, D. J. Hagan and E. W. Van Stryland, *IEEE J. Quantum Electron.,* 1990**, 26**, 760-9.

50 M. R. Rashidian Vaziri, *Appl. Opt*., 2013, **52**, 4843-4848.

51 C. H. Kwak, Y. L. Lee and S. G. Kim, *J. Opt. Soc. Am. B*, 1999, **16**, 600-604.

52 L. Pálfalvi, B. C. Tóth, G. Almási, J. A. Fülöp and J. Hebling, *Appl. Phys. B: Lasers Opt*., 2009, **97**, 679-685.

53 S.-Q. Chen, Z.-B. Liu, W.-P. Zang, J.-G. Tian, W.-Y. Zhou, F. Song, and C.-P. Zhang, *J. Opt. Soc. Am. B,* 2005, **22**, 1911-1916.

54 D. Kovsh, D. Hagan and E. Van Stryland, *Opt. Express,* 1999, **4**, 315-327.

55 S. Cho, J. M. Lim, S. Hiroto, P. Kim, H. Shinokubo, A. Osuka and D. Kim, *J. Am. Chem. Soc.,* 2009**, 131**, 6412-6420.

56 M. Kruk, A. Karotki, M. Drobizhev, V. Kuzmitsky, V. Gael and A. Rebane, *J. Lumin.,* 2003**, 105**, 45-55.

57 M. Morone, L. Beverina, A. Abbotto, F. Silvestri, E. Collini, C. Ferrante, R. Bozio and G. A. Pagani, *Org. Lett.,* 2006**, 8**, 2719-2722.

58 M. Drobizhev, F. Meng, A. Rebane, Y. Stepanenko, E. Nickel and C. W. Spangler, *J. Phys. Chem. B,* 2006**, 110**, 9802-9814.

59 K. Ogawa, A. Ohashi, Y. Kobuke, K. Kamada and K. Ohta, *J. Am. Chem. Soc.,* 2003**, 125**, 13356-13357.

60 D. Swain, P. T. Anusha, T. S. Prashant, S. P. Tewari, T. Sarma, P. K. Panda, S. V. Rao, *Appl. Phys. Lett*., 2012, **100**,141109/1-141109/5.

RSC Advances Accepted Manuscript

This journal is © The Royal Society of Chemistry [year]